Check for updates

*Research Article*

INTERNATIONAL JOURNAL OF ADVANCED ROBOTIC SYSTEMS

*International Journal of Advanced Robotic Systems*
January-February 2018: 1–10
© The Author(s) 2018
DOI: 10.1177/1729881417748126
journals.sagepub.com/home/arx
SAGE

# Design and kinematics analysis of a novel six-degree-of-freedom serial humanoid torso

**Tao Li[1,2], Peng Yao[1,2], Minzhou Luo[2], Zhiying Tan[2], Meiling Wang[1] and Ziyi Guo[1,2]**

**Abstract**

This article presents a bioinspired humanoid torso which is supposed to be used as the trunk for humanoid robots. It can effectively mimic motions of human torso with high degrees of freedom, and it has high stiffness and easy-to-control features. The main structure of the proposed torso is a six-degree-of-freedom serial mechanism with twist angles that are not equal to 0, $\pi/2$ or $\pi$ and zero-length links. Forward kinematic and workspace analysis based on Denavit–Hartenberg and Monte Carlo methods have been formulated to analyze the feasibility of this structure. In addition, a hybrid method combing the large-scale regularity search capabilities of chaos optimization and the quasi-Newton method with relatively high-speed convergence has been proposed to analyze inverse kinematics. Simulations are carried out with the aim to validate the correctness and efficiency of this method for studying the inverse kinematics.

**Keywords**

Humanoid robot, torso, serial robot, kinematics analysis, numerical method

Date received: 25 January 2017; accepted: 9 November 2017

Topic: Humanoid Robotics
Topic Editor: Professor Andrey V Savkin
Associate Editor: Jayantha Katupitiya

## Introduction

The environment of modern society is designed for mankind. For example, the height of staircase, the shape of the driver's seat and the position of the handrail are all designed according to human size and movement. Thus, when designing service robot, it's more economical to develop humanoid robots than to modify the whole environment. This is one main reason that humanoid robots have been widely studied throughout the whole world.

For humanoid robots, legs and arms have been widely studied to realize walking and various operations. However, research of robot torso has been neglected for a long time in the past. Comparing to 1–3 degrees of freedom (DOFs) torsos of most humanoid robots, human torso is a complex system with multiple DOFs related to spine, muscles, brain, and skeleton. It plays an important role in human movements. Most presented humanoid robots[1–5] are weak in aspects of high flexibility and large range of motions due to their oversimplified torso structures with 1–3 DOFs in waist.

[1] Institute of Advanced Manufacturing Technology, Hefei Institutes of Physical Science, Chinese Academy of Sciences, Changzhou, People's Republic of China
[2] Department of Precision Machinery and Precision Instrumentation, University of Science and Technology of China, Hefei, People's Republic of China

**Corresponding author:**
Peng Yao, Institute of Advanced Manufacturing Technology, Hefei Institutes of Physical Science, Chinese Academy of Sciences, Changzhou, 213164, People's Republic of China; Department of Precision Machinery and Precision Instrumentation, University of Science and Technology of China, Hefei, 230022, People's Republic of China.
Email: ypstyle@mail.ustc.edu.cn

Creative Commons CC BY: This article is distributed under the terms of the Creative Commons Attribution 4.0 License (http://www.creativecommons.org/licenses/by/4.0/) which permits any use, reproduction and distribution of the work without further permission provided the original work is attributed as specified on the SAGE and Open Access pages (https://us.sagepub.com/en-us/nam/open-access-at-sage).

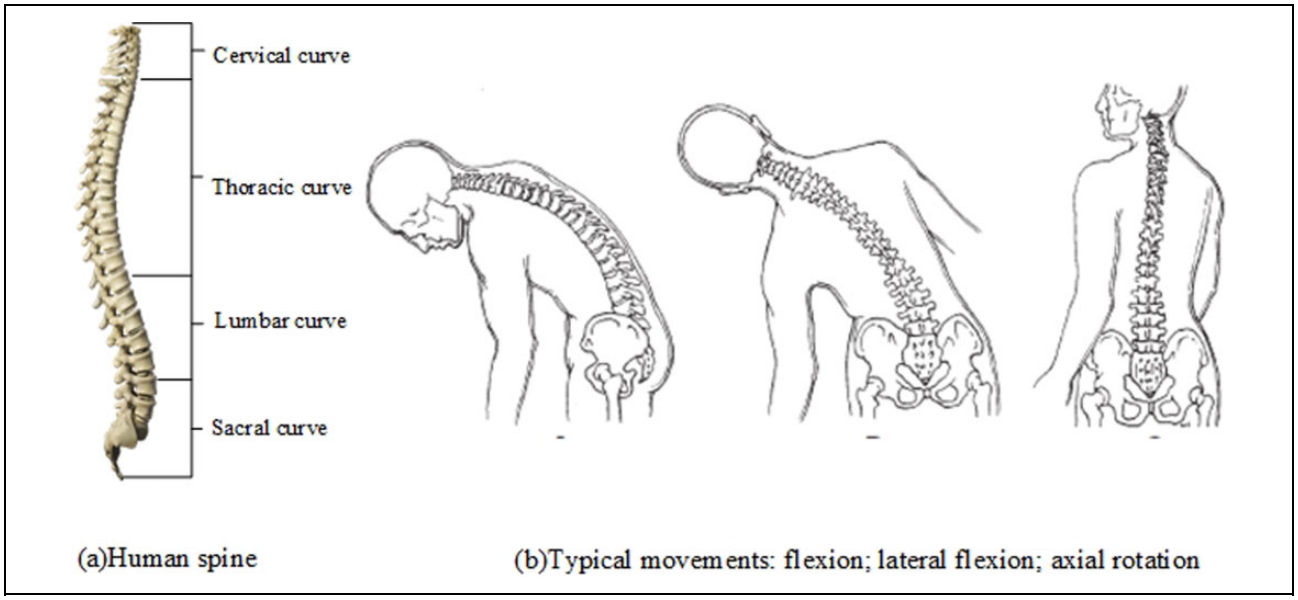


**Figure 1.** Human spine and typical movements of human body.

Recently, some new torso structures of humanoid robots inspired by human torso have been reported. We investigated them and divided them into three main categories: serial, parallel, and hybrid structures. The cable-driven serial torso structures of Kotaro,[6] Kojiro,[7] Kenshiro,[8] and ECCE-3[9] with a large number of artificial muscles have high flexibility and can achieve large-scale bending motions. However, they have poor controllability and low load capacity. The parallel torso is based on a parallel manipulator that consists of a moving platform, a fixed base, and some identical actuated chains. This kind of torso can achieve typical movements of a human body, but the workspace is pretty small compared to serial robots. The hybrid torso structure combines the serial and parallel categories. This type has advantages of the above-mentioned two kinds of structures. However, extra benefits come with extra prices. In addition, kinematics and dynamics analyses are complex issues due to the complicated hybrid structure.

In this article, a new humanoid torso has been proposed based on a special 6-DOF serial mechanism with twist angles that are not equal to 0, $\pi/2$ or $\pi$ and zero-length links with the inspirations of human bionics. The advantages and feasibility of this mechanism have been carried out by kinematics analysis of the proposed torso structure.

The article is organized as follows: "The bioinspired humanoid torso" section introduces the mechanism of the proposed bioinspired humanoid torso. The "forward kinematics and workspace analysis" section clarifies the forward kinematics and workspace. The "inverse kinematics" section presents a detailed explanation of the inverse kinematics process and outlines the hybrid numerical approach. In addition, numerical examples of the proposed torso structure are also illustrated. In the "conclusion" section, the major results of this article are summarized.

## The bioinspired humanoid torso

Human spine features four sagittal curves including cervical, thoracic, lumbar, and sacral curves, as shown in Figure 1(a). Curvature is qualified for the role of keeping the mass center of torso close to the longitudinal axis so that humans can maintain balance. Torsos with curvatures provide more than 10 times of strength and resilience compared with straight vertebral column. Human trunk motions are the result of collaborations between vertebral joints and muscle groups. Due to the flexibilities of these muscle groups, human trunk can withstand large loads. Typical movement patterns of human torso including rotation, flexion (or extension), and lateral bending are shown in Figure 1(b).[10] Motion degrees between adjacent vertebrae are relatively small, but the entire spine with 30 vertebrae in a series shows large workspace.

In Figure 2, the proposed new torso structure is illustrated in a 3-D model in SolidWorks environment and a prototype of 3-D printing is presented. The system consists of six revolute units marked as R1–R6 connected together in series. The six units are divided into two basic modules as shown in Figure 2(c) and (d). Internal components are substantially the same including harmonic reducer, motor, output flange sleeve, input flange cover, actuator, and encoder. The difference is the angle between output flange sleeve and input flange cover, which decides the location of rotation axes and subsequently decides motion results. The design concept begins with the serial mechanism, but it's quite different from presented humanoid torsos. It is based on a general 6-DOFs mechanism with twist angles

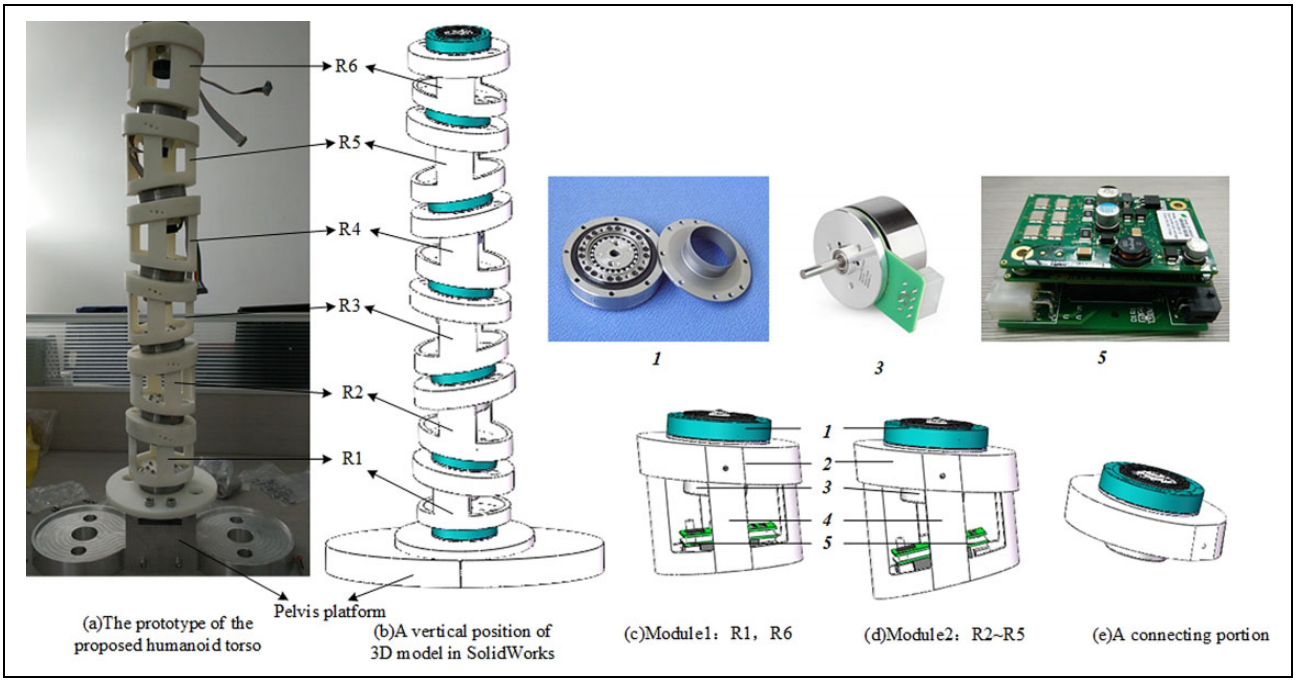


**Figure 2.** (a) and (b): The proposed humanoid torso system; (c) to (e): components of the proposed torso structure: (1) harmonic reducer; (2) input flange cover; (3) disk type motor and encoder; (4) output flange sleeve; (5) motor driver.

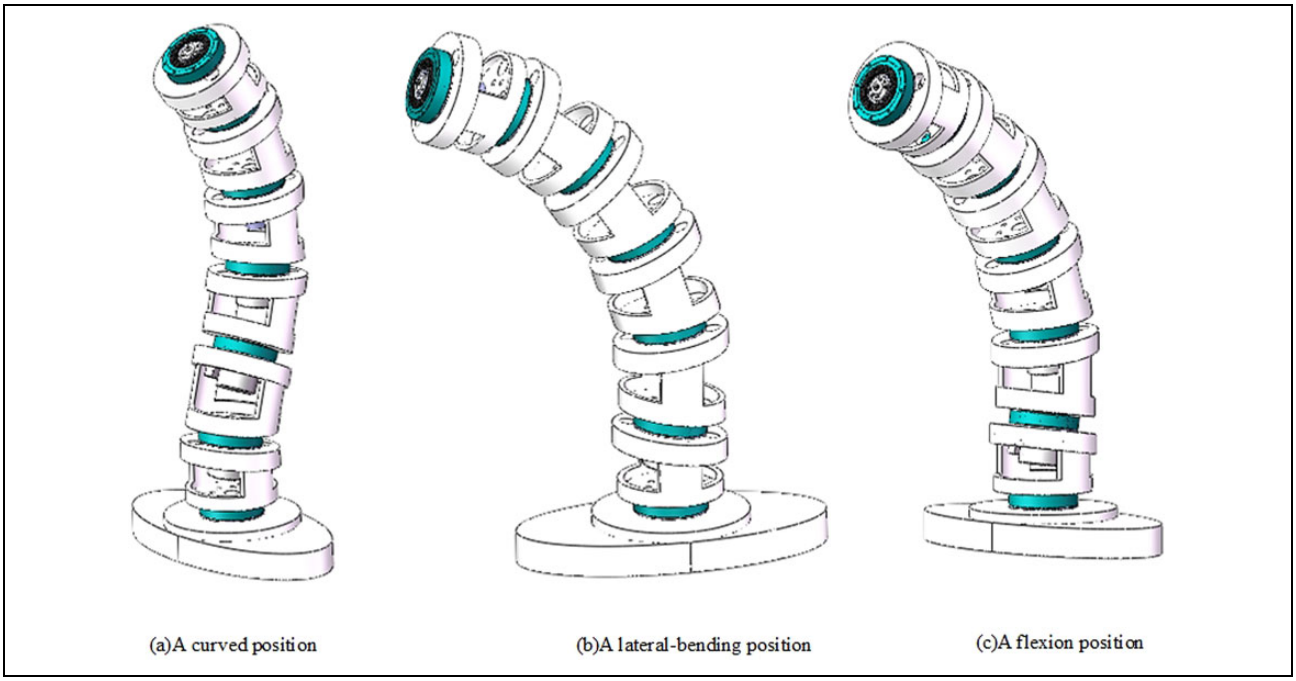


**Figure 3.** Typical motion patterns using humanoid torso.

that are not equal to 0, $\pi/2$ or $\pi$ and zero-length links with the inspirations of human bionics. It's similar to human spine both in shape and functions, and we adopt rigid connection method instead of flexible artificial muscles for considerations of load capacity and controllability as discussed above.

The motion principle of this humanoid torso using disk type actuators is quite different from human spine's skeleton–muscles motion methods. Independent motions of six units controlled by six actuators result in coupling motion types. Typical motion patterns can be achieved: Figure 3(a) shows the imitation of physiological curvature of the spine

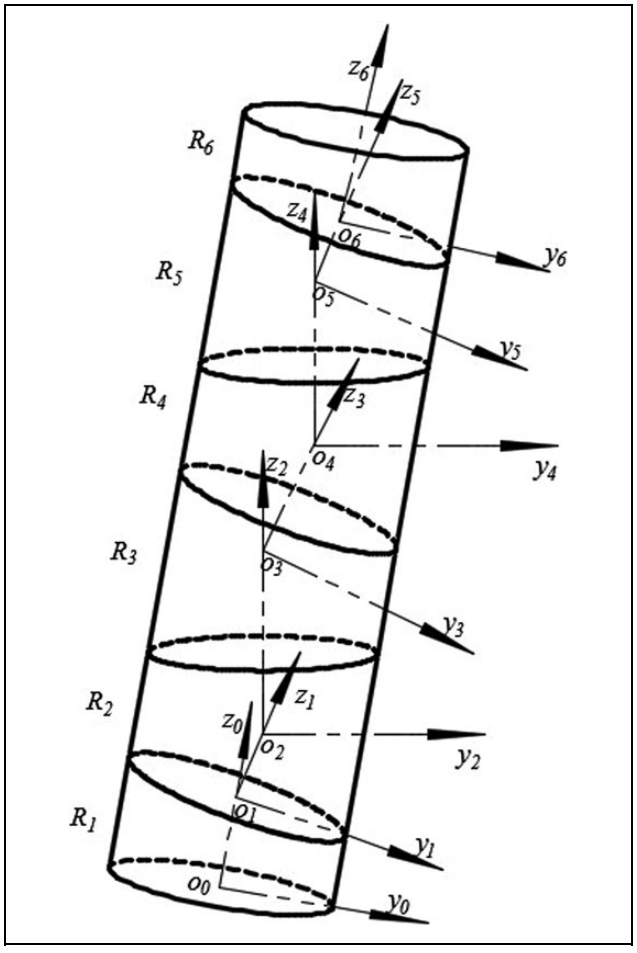


**Figure 4.** Configurations of the proposed humanoid torso with D–H system. D–H: Denavit–Hartenberg.

and Figure 3(b) and (c) shows the actions of lateral bending and flexion.

## Forward kinematics and workspace analysis

The configuration of the proposed humanoid torso, as shown in Figure 4, consists of six units. Four Denavit–Hartenberg (D–H) parameters associated with a particular convention for attaching reference frames to the proposed torso structure are also shown in Figure 4 and Table 1; the $x$-axis follows the $y$-axis and $z$-axis by choosing it to be a right-handed coordinate system.

The homogeneous transformation matrix is

$$\boldsymbol{A}_i = \begin{bmatrix} \cos\theta_i & -\sin\theta_i \sin\alpha_i & \sin\theta_i \sin\alpha_i & a_{i-1}\cos\theta_i \\ \sin\theta_i & \cos\theta_i \cos\alpha_i & -\cos\theta_i \sin\alpha_i & a_{i-1}\sin\theta \\ 0 & \sin\alpha_i & \cos\alpha_i & d_i \\ 0 & 0 & 0 & 1 \end{bmatrix} \tag{1}$$

where $\theta_i$ is a joint angle at joint $i$,$\alpha_i$ is a twist angle, $a_i$ is a link length, and $d_i$ is an offset at joint $i$

**Table 1.** D–H parameters.

| # | $\theta$ (°) | $d$ (mm) | $a$ (mm) | $\alpha$ |
|---|---|---|---|---|
| 0–R1 | $\theta_1$ | 100.6 | 0 | −8.3° |
| R1–R2 | $\theta_2$ | 45.9 | 0 | 16.6° |
| R2–R3 | $\theta_3$ | 91.8 | 0 | −16.6° |
| R3–R4 | $\theta_4$ | 91.8 | 0 | 16.6° |
| R4–R5 | $\theta_5$ | 91.8 | 0 | −16.6° |
| R5–R6 | $\theta_6$ | 45.9 | 0 | 8.3° |

D–H: Denavit–Hartenberg.

$$^0\boldsymbol{T}_6 = \boldsymbol{A}_1\boldsymbol{A}_2\boldsymbol{A}_3\boldsymbol{A}_4\boldsymbol{A}_5\boldsymbol{A}_6 = \begin{bmatrix} n_x & o_x & a_x & p_x \\ n_y & o_y & a_y & p_y \\ n_z & o_z & a_z & p_z \\ 0 & 0 & 0 & 1 \end{bmatrix} = \begin{bmatrix} \boldsymbol{n} & \boldsymbol{o} & \boldsymbol{A} & \boldsymbol{p} \\ 0 & 0 & 0 & 1 \end{bmatrix} \tag{2}$$

where $\boldsymbol{n}$, $\boldsymbol{o}$, $\boldsymbol{A}$, and $\boldsymbol{p}$ represent the pose of the end effector.

However, it's not clear whether the proposed new humanoid torso based on a special 6-DOFs mechanism could achieve continuous typical motion actions in Cartesian space. As shown in Figure 5, workspace of the proposed torso mechanism has been analyzed using Monte Carlo method[11,12] based on forward kinematics. Monte Carlo method has no limits to joint types and ranges of joint variables; it uses $\theta_i = \theta_i{}^{\min} + (\theta_i{}^{\max} - \theta_i{}^{\min}) \times \text{Rand}()$ in $[-\pi, \pi]$ to generate values of joints, where Rand() is a uniform pseudo-random number. It can be seen that the shape of the proposed torso structure's workspace is part of a sphere with smooth and uniform surface, so for a humanoid robot, the end effector (the head) of the torso mechanism could move along the trajectory from A to B in Cartesian space to imitate lateral bending or the trajectory from A to C in Cartesian space to imitate flexion. It can be demonstrated theoretically from above analysis that continuous trajectory planning in Cartesian space to achieve typical movements is feasible.

## Inverse kinematics

Typical inverse kinematic methods include analytical method and numerical method. Analytical method is quite superior when the mechanism satisfies the Piper criterion. Otherwise, this method becomes complex when it involves in general 6-DOFs serial manipulators in terms of producing extraneous roots and ill-conditioned matrices. So, numerical method becomes the only way to be considered due to the characteristic of the proposed torso structure. Numerical methods mainly include iterative methods and optimization-based methods, and they are consistent in some aspects. Typical iterative method based on Newton–Raphson algorithm is widely used to solve inverse kinematics for serial robots. However, it's very sensitive to initial iteration

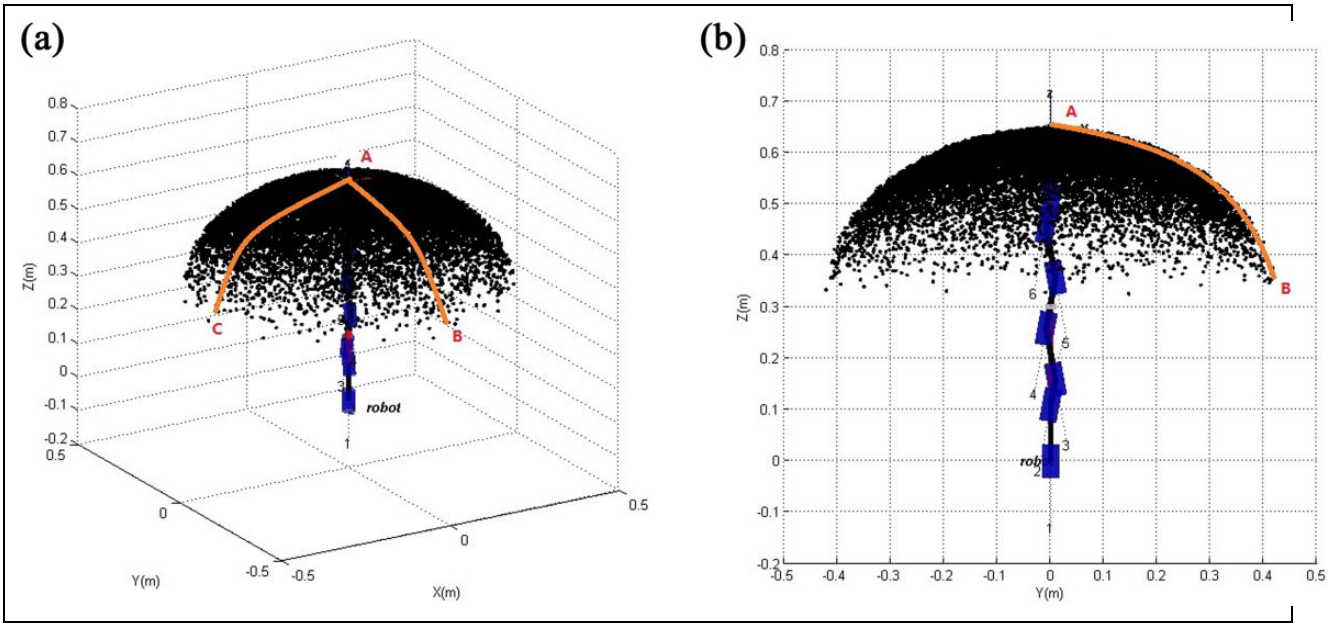


**Figure 5.** Workspace analysis.

values, which means that robots are easy to fall into the near-singular state and then lead to wrong values.[13]

## *An optimization-based equation for inverse kinematics*

In this article, optimization-based methods become the ideal way to be considered. Inverse kinematic is analyzed by the process of solving $\theta_1 - \theta_6$ with four known D–H symbols. The basic matrix equation can be transformed into the new form[14–16]

$$A_3 A_4 A_5 = {A_2}^{-1} {A_1}^{-1} {}^0T_6 {A_6}^{-1} \tag{3}$$

The new matrix reduces the analytical complexity of equation (2) because the joint angle $\theta_6$ is excluded in the third and fourth columns of both sides for the features of $A_6^{-1}$. Equation (3) is expanded as follows

$$\begin{bmatrix} n_{11}(\theta_3,\theta_4,\theta_5) & o_{12}(\theta_3,\theta_4,\theta_5) & a_{13}(\theta_3,\theta_4,\theta_5) & p_{14}(\theta_3,\theta_4,\theta_5) \\ n_{21}(\theta_3,\theta_4,\theta_5) & o_{22}(\theta_3,\theta_4,\theta_5) & a_{23}(\theta_3,\theta_4,\theta_5) & p_{24}(\theta_3,\theta_4,\theta_5) \\ n_{31}(\theta_3,\theta_4,\theta_5) & o_{32}(\theta_4,\theta_5) & a_{33}(\theta_4,\theta_5) & p_{34}(\theta_4,\theta_5) \\ 0 & 0 & 0 & 1 \end{bmatrix} = \begin{bmatrix} {n_{11}}'(\theta_1,\theta_2,\theta_6) & {o_{12}}'(\theta_1,\theta_2,\theta_6) & {a_{13}}'(\theta_1,\theta_2) & {p_{14}}'(\theta_1,\theta_2) \\ {n_{21}}'(\theta_1,\theta_2,\theta_6) & {o_{22}}'(\theta_1,\theta_2,\theta_6) & {a_{23}}'(\theta_1,\theta_2) & {p_{24}}'(\theta_1,\theta_2) \\ {n_{31}}'(\theta_1,\theta_2,\theta_6) & {o_{32}}'(\theta_1,\theta_2,\theta_6) & {a_{33}}'(\theta_1,\theta_2) & {p_{34}}'(\theta_1,\theta_2) \\ 0 & 0 & 0 & 1 \end{bmatrix} \tag{4}$$

As the next step, substitution using the trigonometric relations is done to make a clear expression

$$\begin{aligned} &x_1 = \sin\theta_1, \quad x_2 = \cos\theta_1, \quad x_3 = \sin\theta_2, \quad x_4 = \cos\theta_2 \\ &x_5 = \sin\theta_3, \quad x_6 = \cos\theta_3, \quad x_7 = \sin\theta_4, \quad x_8 = \cos\theta_4 \\ &x_9 = \sin\theta_5, \quad x_{10} = \cos\theta_5, \quad x_{11} = \sin\theta_6, \quad x_{12} = \cos\theta_6 \end{aligned} \tag{5}$$

since the values of third and fourth columns in equation (5) on both sides are not associated with $\theta_6$. Six equations extracted from the third and fourth columns in equation (4) can be obtained after multiplied by the transformations in equation (6)

$$\begin{cases} f_1(x_1,x_2,\cdots,x_{10}) = a_{13} - {a_{13}}' & f_4(x_1,x_2,\cdots,x_{10}) = p_{14} - {p_{14}}' \\ f_2(x_1,x_2,\cdots,x_{10}) = a_{23} - {a_{23}}' & f_5(x_1,x_2,\cdots,x_{10}) = p_{24} - {p_{24}}' \\ f_3(x_1,x_2,\cdots,x_{10}) = a_{33} - {a_{33}}' & f_6(x_1,x_2,\cdots,x_{10}) = p_{34} - {p_{34}}' \end{cases} \tag{6}$$

At this point, trigonometric relation $\sin^2\theta_i + \cos^2\theta_i = 1$ ($i = 1$–$6$) is used to get six new equations considering the substitutions in equation (5)[16,17]

$$\begin{cases} f_7 = {x_1}^2 + {x_2}^2 - 1 & f_{10} = {x_7}^2 + {x_8}^2 - 1 \\ f_8 = {x_3}^2 + {x_4}^2 - 1 & f_{11} = {x_9}^2 + {x_{10}}^2 - 1 \\ f_9 = {x_5}^2 + {x_6}^2 - 1 & f_{12} = {x_{11}}^2 + {x_{12}}^2 - 1 \end{cases} \tag{7}$$

The benefit of using trigonometric equation is that the range of the variables is restricted within $(-1, 1)$ during the iteration procedure. It can guarantee to obtain meaningful solutions.

Consequently, the inverse kinematic solution of the proposed torso structure is equivalent to solve the minimum values of a master equation described as follows:

$$\begin{cases} \text{Min}: \quad F(\boldsymbol{x}) = \sum_{i=1}^{11} f_i^2(\boldsymbol{x}) \\ \boldsymbol{x} = (x_1, x_2, \cdots, x_{10})^{\mathrm{T}}, \boldsymbol{x} \in [-1, 1] \end{cases} \tag{8}$$

## Hybrid numerical approach of Chaos-BFGS method

In this section, a hybrid method combing the large-scale regularity search capabilities of chaos optimization and high-speed convergence of quasi-Newton method has been proposed to solve inverse kinematics.

*The BFGS algorithm.* Newton's method is one of the most widely used algorithms for optimization. The basic iterative formula is summarized below

$$\boldsymbol{x}^{(k+1)} = \boldsymbol{x}^{(k)} - \boldsymbol{H}(x^{(k)})^{-1}\nabla f(\boldsymbol{x}^{(k)}) \tag{9}$$

where $\nabla f(\boldsymbol{x}^{(\mathrm{k})})$ is the gradient and $\boldsymbol{H}(x^{(k)})$ is the Hessian matrix.

Newton's method has its own disadvantages such as sensibility to the initial iterative value, inability to ill-conditioned matrix, and time cost for Jacobian matrix. BFGS quasi-Newton method revised the disadvantages by using an approximation matrix $\boldsymbol{B}_k$ to replace $\boldsymbol{H}(x^{(k)})^{-1}$ and determines the value of the iterative step size by $\alpha_k = \arg\min f\left(\boldsymbol{x}^{(k)} - \boldsymbol{H}\left(x^{(k)}\right)^{-1}\nabla f\left(\boldsymbol{x}^{(k)}\right)\right)$.[18] Hence, the modified formula is

$$\boldsymbol{x}^{(k+1)} = \boldsymbol{x}^{(k)} - \alpha_k \boldsymbol{B}_k \nabla f(\boldsymbol{x}^{(k)}) \tag{10}$$

$$\boldsymbol{B}_{k+1} = \boldsymbol{B}_k + \left(1 + \frac{\left(\Delta \boldsymbol{g}^{(k)}\right)^{\mathrm{T}} \boldsymbol{B}_k \Delta \boldsymbol{g}^{(k)}}{\left(\Delta \boldsymbol{g}^{(k)}\right)^{\mathrm{T}} \Delta \boldsymbol{x}^{(k)}}\right) \frac{\Delta \boldsymbol{x}^{(k)} (\Delta \boldsymbol{x}^{(k)})^{\mathrm{T}}}{(\Delta \boldsymbol{x}^{(k)})^{\mathrm{T}} \Delta \boldsymbol{g}^{(k)}} - \frac{\boldsymbol{B}_k \Delta \boldsymbol{g}^{(k)} (\Delta \boldsymbol{x}^{(k)})^{\mathrm{T}} + (\boldsymbol{B}_k \Delta \boldsymbol{g}^{(k)} (\Delta \boldsymbol{x}^{(k)})^{\mathrm{T}})^{\mathrm{T}}}{(\Delta \boldsymbol{g}^{(k)})^{T} \Delta \boldsymbol{x}^{(k)}} \tag{11}$$

where

$$\begin{cases} \boldsymbol{g}^{(k)} = \nabla f(\boldsymbol{x}^{(k)}) \\ \Delta \boldsymbol{g}^{(k)} = \nabla f(\boldsymbol{x}^{(k+1)}) - \nabla f(\boldsymbol{x}^{(k)}) \\ \Delta \boldsymbol{x}^{(k)} = \boldsymbol{x}^{(k+1)} - \boldsymbol{x}^{(k)} \end{cases} \tag{12}$$

Quasi-Newton methods can achieve superlinear convergence if the initial iteration point is close to the solution. However, it's not always effective in solving the minimum of multidimensional nonlinear equations for getting local extremum if the initial guess is not sufficiently close to the solution, or if singular points are encountered.[19] In other words, these methods are locally convergent and provide no guarantee for obtaining solutions. Some methods have been tried to overcome the disadvantages, but the extra benefits come with extra prices,[20,21] effects are not good.

*Chaos optimization method.* Chaos is a highly unstable motion of deterministic systems in finite phase space.[22] Logistic chaotic equations are used to generate chaotic variables for optimal searching[23]

$$x_{n+1} = \mu x_n (1 - x_n) \tag{13}$$

where $\mu$ is a control parameter and $n = 0, 1, 2\ldots$. Suppose $0 \le x_0 \le 1$, when $\mu \in [3.56, 4]$, the logistic system becomes chaotic. The logistic system is based on the properties of ergodicity, stochastic, and 'regularity' of chaos. When $n$ variables are optimized, $n$ different values belong to (0, 1) are set for the initial values and ensure that these values are not equal to fixed points 0, 0.25, 0.75, 1. So, $n$ chaotic variables with different trajectories can be obtained.[24] Chaos optimization method can search global extremum on regularity of chaotic motion quickly; however, it lacks local convergence ability.

*Chaos-BFGS method.* In combination with the advantages of two algorithms, theoretically, the hybrid approach of chaos-BFGS method can effectively avoid the local extremum traps when the BFGS method is used to calculate the extreme value of the high-dimensional sub-nonlinear equation. The main steps are summarized below:

- *Step 1*: Set the solution error $\varepsilon$, run the chaos optimization algorithm to solve the systems of nonlinear equations described in equation (8).
- *Step 2*: Make the current solutions $\boldsymbol{x}^*$ obtained by the chaos optimization algorithm as the initial vector to the BFGS method, then solve the high-dimensional sub-nonlinear equation and get the solution $\boldsymbol{x}^{**}$, set $\boldsymbol{x}^* = \boldsymbol{x}^{**}$.
- *Step 3*: If $F(\boldsymbol{x}^*) < \varepsilon$, the hybrid algorithm is terminated; else, make $\boldsymbol{x}^*$ as the initial vector of chaotic search, go back to *step 1*.

In the chaos-BFGS method, chaos optimization algorithm is used to explore the solution space and locate the global initial solution of the system of nonlinear equation for the BFGS algorithm to avoid the local minimum. While the BFGS method is used to obtain the exact solution of the high-dimensional sub-nonlinear equation, the chaos-BFGS method includes the global search capabilities of the chaos

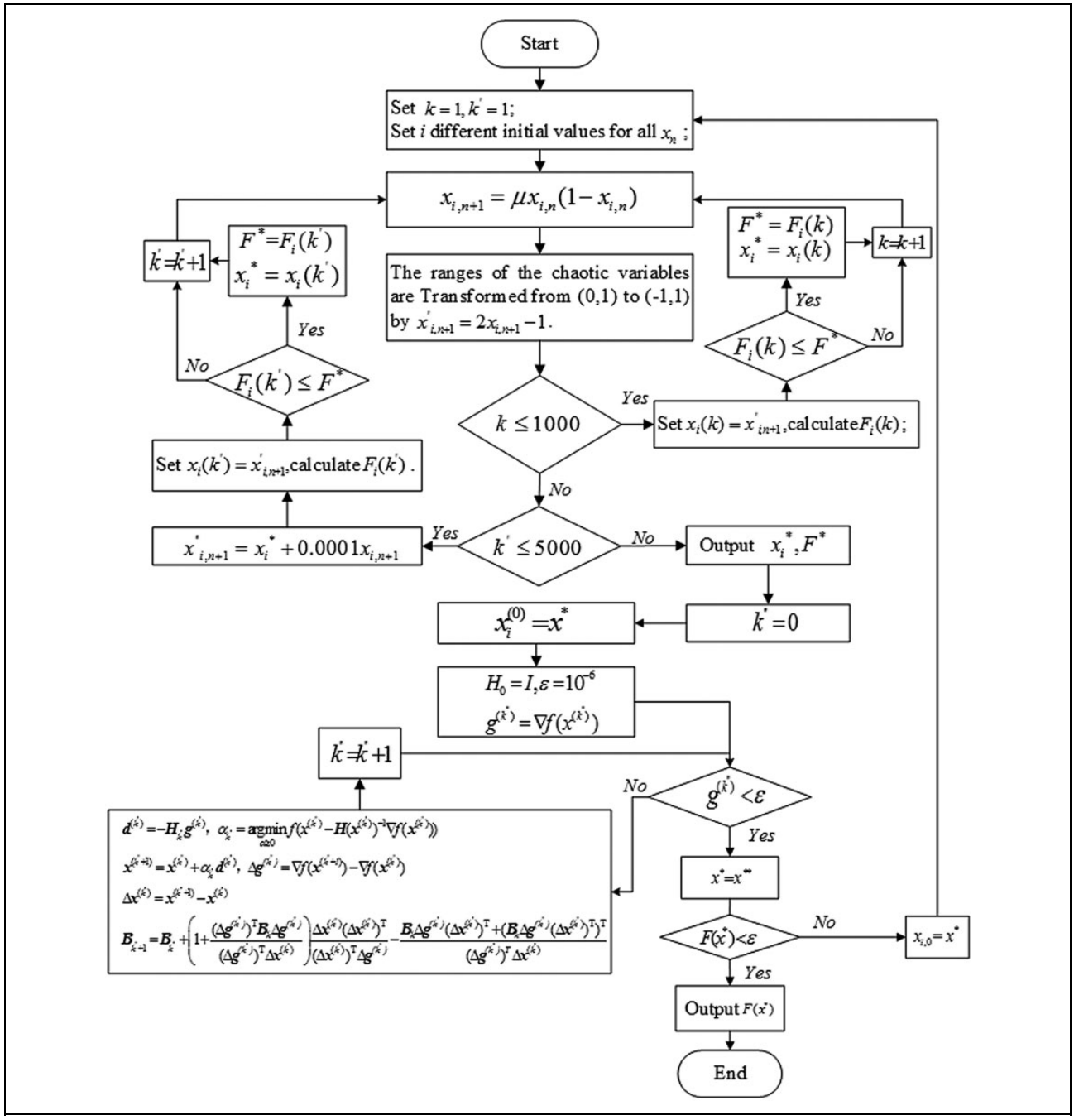


**Figure 6.** Flowchart of chaos-BFGS method; BFGS: Broyden-Fletcher-Goldfarb-Shanno.

optimization and the high local convergence rate of the BFGS quasi-Newton method, so the hybrid approach has excellent performance in theory compared to other methods.

## *Numerical examples and discussions*

A 4 × 4 homogeneous matrix of the proposed torso structure's pose derived from forward kinematics using an arbitrarily selected joint angles is as follows

$$T=\begin{bmatrix} 0.996576403552939 & 0.079360147236245 & -0.023182728746453 & 0.047841138261263 \\ -0.079360147236245 & 0.839595602678195 & -0.537383653448893 & -0.149366870349598 \\ -0.023182728746452 & 0.537383653448893 & 0.843019199125256 & 0.560221681406954 \\ 0 & 0 & 0 & 1 \end{bmatrix} \quad (14)$$

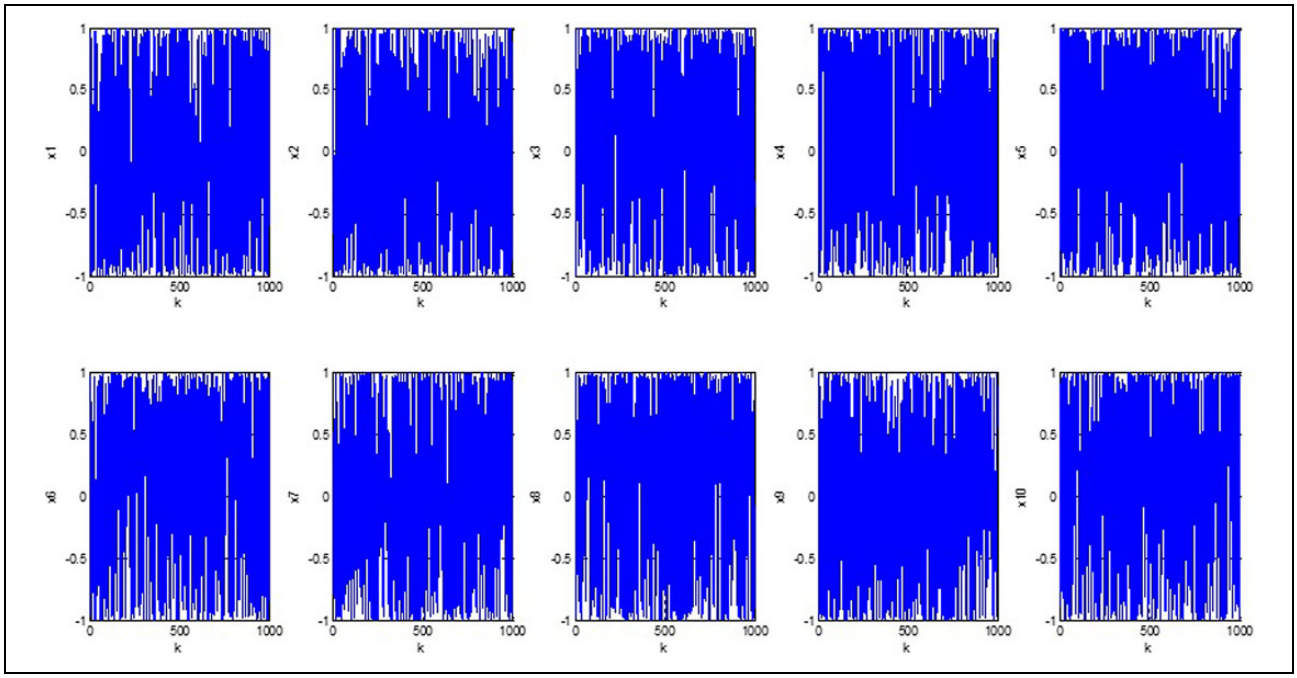


**Figure 7.** The logistic map chaotic generator spectrum of $x_1 - x_{10}$.

At first, the chaos optimization is used to find the initial vector for the BFGS algorithm. Consider that $\theta \in [-\pi, \pi]$, so $x_i \in [-1, 1]$. Set the allowable error $\varepsilon = 10^{-6}$. Set the first chaotic iterative steps as 1000 and the second carrier chaotic iterative steps as 5000. The values of variables $x_1 - x_{10}$ and the main equation $F(\boldsymbol{x})$ during the iterative process are shown in Figures 7 and 8.

It can be seen that the values of $x_1 - x_{10}$ effectively traversed the value range after the second carrier iteration. The initial point of the BFGS algorithm, which is the closest to the global optimal point, is obtained: [0.9994, 0.1547, 0.9350, 0.3262, 0.2020, 0.9576, 0.6368, 0.7712, 0.9666, 0.1772].

Take this point as the initial vector, the BFGS algorithm finds one of the exact solutions with 32 steps, as shown in Figure 9(a): [−0.1498, 0.0734, −0.1142, −0.0848, 0.0380, −0.4037, −0.0274, −0.1315, 0.0033, 0.0020]. The value of $F(\boldsymbol{x})$ is $3.9829 \times 10^{-9}$ when the value of $g^{(32)}$ reaches the stopping criterion. Corresponding joint angles $\theta_1 - \theta_6$ can be calculated: [−1.6968, 1.5938, −0.1911, 0.5347, 1.7548, −2.1197] rad by using $\theta_i = \arctan(x_m / x_{m+1})$ ($i$ = 1–6, $m$ = 1–11).

In Figure 9(b), the BFGS method with an arbitrarily selected initial vector$^{0,0,0,0,0,0,0,0,0,0}$ gets the solution $5.5495 \times 10^{-6}$ of $F(\boldsymbol{x})$ taking over 350 iterative steps. In Figure 9(c), the iterative error of the Jacobian method with an initial value$^{0,0,0,0,0,0}$ in Robotics Toolbox reaches about 0.064, warning occurs that initial joint configuration results a near-singular configuration and this may slow convergence when the algorithm is running. It can be calculated that the rank of the Jacobian matrix is six in this case, which is not in the singular state. In fact, other arbitrary initial values could also result in this warning after many numerical experiments.

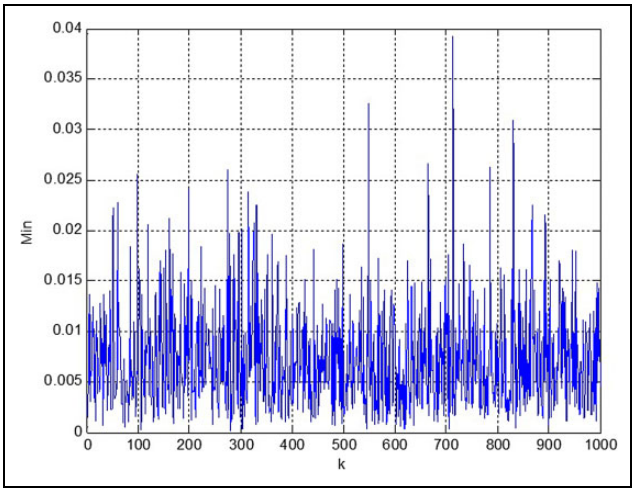


**Figure 8.** The logistic map chaotic generator spectrum of $F(\boldsymbol{x})$.

The concept of manipulability can be used to explain this problem. Consider the set of joint velocities with a unit norm

$$\dot{\boldsymbol{q}}^{\mathrm{T}} \dot{\boldsymbol{q}} = 1 \tag{15}$$

where $\dot{\boldsymbol{q}}$ are joint velocities, which lie on the surface of a hypersphere in the six-dimensional joint velocity space. Substituting equation (16), it can be written as equation (17)

$$\dot{\boldsymbol{q}} = \boldsymbol{J}(\boldsymbol{q})^{-1} \boldsymbol{v} \tag{16}$$

$$\boldsymbol{v}^{\mathrm{T}} (\boldsymbol{J}(\boldsymbol{q}) \boldsymbol{J}(\boldsymbol{q})^{\mathrm{T}})^{-1} \boldsymbol{v} = 1 \tag{17}$$

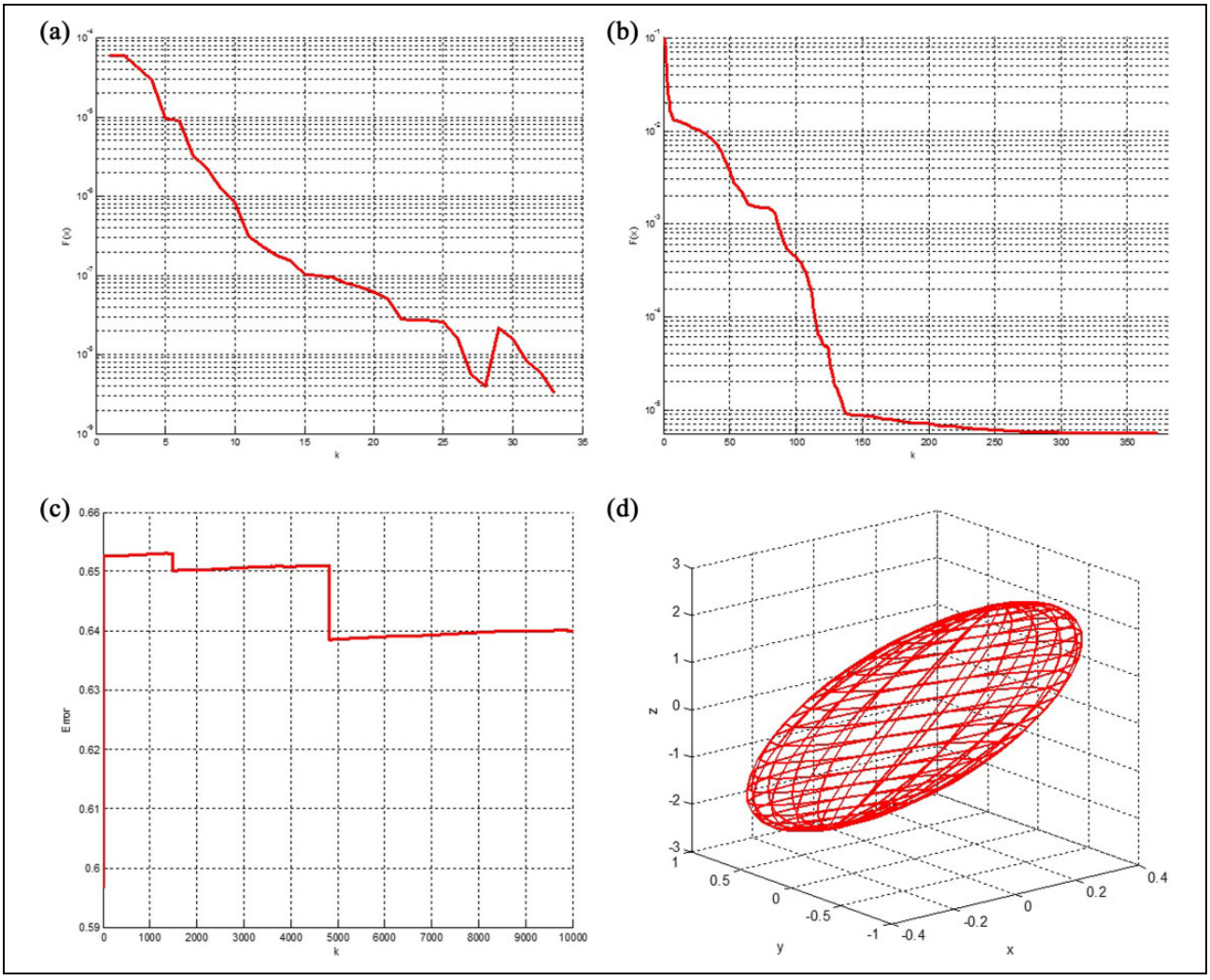


**Figure 9.** Error of three iterative methods: (a) chaos-BFGS method; (b) BFGS method with an initial value [0,0,0,0,0,0,0,0,0,0]; (c) Jacobian method with an initial value [0,0,0,0,0,0] in MATLAB Robotics Toolbox; (d) rotational velocity ellipsoid of the numerical case.

where $\boldsymbol{v}$ represents velocities of end effector and $\boldsymbol{J}(\boldsymbol{q})$ is the Jacobian matrix. Equation (17) is the equation of points on the surface of a six-dimensional ellipsoid in the end-effector velocity space. If this ellipsoid is close to spherical, that is, its radii are of the same order of magnitude, then all is well—the end effector can achieve arbitrary Cartesian velocity. However, if one or more radii are very small, this indicates that the end effector can't achieve velocity in the directions corresponding to those small radii.[25] It can be seen from the rotational velocity ellipsoid of the numerical examples, as shown in Figure 9(d), that the end effector can achieve much higher velocity in the $z$-direction than in the $x$- and $y$-directions, which indicates that the arbitrary chosen pose and orientation are in the near-singular state.

## Conclusions

The characteristics of the proposed bioinspired humanoid torso based on a general 6-DOF serial mechanism with twist angles that are not equal to 0, $\pi/2$ or $\pi$ and zero-length links have been investigated. Forward kinematic based on D–H method and workspace analysis based on Monte Carlo method are implemented to demonstrate that continuous trajectory planning in Cartesian space to achieve typical movements is feasible, which means the new humanoid torso has the ability to achieve typical human postures. As the hybrid chaos-BFGS method has global search ability, the numerical simulations prove that chaos-BFGS method is more effective to solve inverse kinematics in terms of accuracy and speed compared with Newton-type methods under the circumstance that the nonlinear equation is non-smooth and sensitive to the value of initial guess caused by the structural characteristics. The proposed method also can be applied to inverse kinematics of general 6-DOFs serial robots, especially when there are many (near-)singular points caused by special structures. Experimental analyses are to be further investigated to show the feasibility of achieving typical postures by accelerating the construction of experimental platform.

## Acknowledgements

The authors would like to thank Dr Hongbo Zhu for the valuable discussions with them.

## Declaration of conflicting interests

The author(s) declared no potential conflicts of interest with respect to the research, authorship, and/or publication of this article.

## Funding

The author(s) disclosed receipt of the following financial support for the research, authorship, and/or publication of this article: This work was supported by the National Natural Science Foundation of China (grant nos. 51405469, 61401437).

## References

1. Hirose M.Development of humanoid robot ASIMO. In: *IEEE/RSJ international conference on intelligent robots and systems (IROS)*, Maui, USA, 29 October 2001, pp. 1–6.
2. Kim JY, Park IW, Lee J, et al. System design and dynamic walking of humanoid robot khr-2. In: *IEEE international conference on robotics and automation (ICRA)*, Barcelona, Spain, 18–22 April 2005, pp. 1443–1448.
3. Park IW, Kim JY, Lee J, et al. Mechanical design of the humanoid robot platform, HUBO. *Adv Robot* 2007; 21(11): 1305–1322.
4. Ogura Y, Aikawa H, Shimomura K, et al. Development of a new humanoid robot WABIAN-2. In: *IEEE international conference on robotics and automation*, Orlando, USA, 15–19 May 2006, pp. 76–81.
5. Siedel T, Hild M and Weidner M. Concept and design of the modular actuator system for the humanoid robot MYON. In: *International conference on intelligent robotics and applications (ICIRA)*, Aachen, Germany, 6–8 December 2011, pp. 388–396.
6. Mizuuchi I. A musculoskeletal flexible-spine humanoid Kotaro aiming at the future in 15 years' time. In: *Mobile robots: towards new applications*. New York: INTECH Open Access Publisher, 2006, pp. 45–56.
7. Mizuuchi I, Nakanishi Y, Sodeyama Y, et al. An advanced musculoskeletal humanoid Kojiro. In: *IEEE-RAS international conference on humanoid robots*, Pittsburgh, USA, 29 November–1 December 2007, pp. 294–299.
8. Asano Y, Mizoguchi H, Kozuki T, et al. Lower thigh design of detailed musculoskeletal humanoid "Kenshiro". In: *IEEE/RSJ international conference on intelligent robots and systems*, Vilamoura, Portugal, 7–12 October 2012, pp. 4367–4372.
9. Potkonjak V, Svetozarevic B, Jovanovic K, et al. The puller-follower control of compliant and noncompliant antagonistic tendon drives in robotic system. *Int J Adv Robot Syst* 2012; 8: 143–155.
10. Yao P, Li T, Luo MZ, et al. Analysis of human spine functionality from the perspective of humanoid robots. In: *IEEE international conference on mechatronics and automation*, Harbin, China, 7–10 August 2016, pp. 1167–1172.
11. Peidró A, Gil A, Marín JM, et al. Monte-Carlo workspace calculation of a serial-parallel biped robot. In: *Robot 2015: second Iberian robotics conference*, Lisbon, Portugal, 19–21 November 2015, pp. 157–169. Springer, Cham, Switzerland: Advances in Intelligent Systems and Computing, Springer International Publishing.
12. Yao P, Li T, Luo MZ, et al. Mechanism design of a humanoid robotic torso based on bionic optimization. *Int J Humanoid Robot* 2017; 14: 21.
13. Kajita S. *Humanoid robots*. Beijing: Tsinghua University Press, 2007.
14. Manocha D and Canny JF. Real time inverse kinematics for general 6R manipulators. In: *Proceedings of international conference of robotics and automation*, Nice, France, 12–14 May 1992, pp. 383–389.
15. Raghavan M and Roth B. Kinematic analysis of the 6R manipulator of general geometry. In: *Proceeding 5th international symposium on robotics research*, Massachusetts, USA, 1989, pp. 263–269. Cambridge: Cambridge MIT Press.
16. Murray RM, Li Z, and Sastry SS. *A mathematical introduction to robotic manipulator*. Beijing: Machinery Industry Press, 1994.
17. Luo YX, Yi W, and Liu QY. Inverse displacement analysis of a general 6R manipulator based on the hyper-chaotic least square method. *Int J Adv Robot Syst* 2012; 9: 1–6.
18. Chong EKP and Żak SH. *An introduction to optimization*, 4th ed. UK: Wiley, 2013.
19. Luo YZ, Tang GJ, and Zhou LN. Hybrid approach for solving systems of nonlinear equations using chaos optimization and quasi-Newton method. *Appl Soft Comput* 2008; 8(2): 1068–1073.
20. Karr CL, Weck B, and Freeman LM. Solutions to systems of nonlinear equations via a genetic algorithm. *Eng Appl Artif Intell* 1998; 11(3): 369–375.
21. Nocedal J and Wright S. *Numerical optimization*. New York, USA: Springer Science & Business Media, 2006.
22. Yang DX, Li G, and Cheng GD. On the efficiency of chaos optimization algorithms for global optimization. *Chaos Solitons Fractals* 2007; 34(4): 1366–1375.
23. Li SY. *Intelligent optimization algorithm theory and application*. Harbin: Harbin Institute of Technology Press, 2012.
24. Li B and Jiang W S. Chaos optimization method and its application. *Control Theory Appl* 1997; 14(4): 613–615.
25. Peter C. *Robotics, vision & control: fundamental algorithms in MATLAB*. Berlin: Springer, 2011.